https://doi.org/10.5194/nhess-2024-92
Preprint. Discussion started: 12 June 2024

Natural Hazards and Earth System Sciences
Discussions

Conversion relationships between Modified Mercalli Intensity and Peak Ground Acceleration for historical shallow crustal earthquakes in Mexico

Quetzalcoatl Rodríguez-Pérez[1,2], F. Ramón Zúñiga[2]

[1] Consejo Nacional de Humanidades, Ciencia y Tecnología, Mexico City, Mexico.
[2] Instituto de Geociencias, Universidad Nacional Autónoma de México, Juriquilla, Querétaro, Mexico.

Correspondence: Quetzalcoatl Rodríguez-Pérez (quetza@geociencias.unam.mx)

Abstract. New empirical relationships between modified Mercalli intensity (MMI) and synthetic peak ground acceleration (PGA) are developed for shallow crustal earthquakes in Mexico. Ground motion data from 18 moderate-to-large earthquakes ($4.5 < M_W < 7.5$) and the corresponding 531 MMI information reports were employed. Synthetic PGA data were generated using the finite-fault stochastic method considering different rupture scenarios in order to extend the limitations of the dataset. Linear and bilinear regression techniques were used considering a binning averaging procedure and the whole dataset. On one hand, a set of MMI predictive equations independent of moment magnitude (M_W) and hypocentral distance (R) were derived. Despite weak dependencies of the residuals on M_W and R terms, on the other hand, we also developed refined predictive relationships that include these parameters as independent variables. The refined PGA to MMI conversion equations show slightly less variability than simple linear equations in predicting intensity values. The proposed predictive equations are consistent with similar relationships in other regions of the world. The discrepancies among the different relationships may reflect the differences in input data, particularly related to the macroseismic intensity assignments, which are inherently subjective, and the tectonic regime. The proposed relationships can be used for improved hazard assessments in Mexico.

https://doi.org/10.5194/nhess-2024-92
Preprint. Discussion started: 12 June 2024

Natural Hazards and Earth System Sciences
Discussions

1 Introduction

Seismic intensity is a measurement that describes the degree of shaking or damage at a particular site. Usually, seismic intensity is represented spatially by intensity maps. These maps provide shaking patterns reflecting earthquake damage and its effects on human dwelings from a specific earthquake. The intensity scale was originally designed to describe and quantify seismic damage in the absence of instrumental recordings. Arguably, one of the first attempts to describe effects of earthquake shaking on a map which led to the development of the intensity scales, was carried out by Mallet (1862). Several intensity scales have been proposed throughout time, for example, the European Macroseismic Scale, the Japan Meteorological Agency seismic intensity scale (JMA), the China Seismic Intensity Scale, the Mercalli-Cancani-Sieberg scale, and the Modified Mercalli Intensity scale (MMI). MMI is currently the most widely used scale worldwide. MMI quantifies the effects of an earthquake using 12 degrees, with 1 indicating not felt and 12 as complete destruction (Wood and Neumann, 1931). The intensity values vary with the distance to the earthquake source, with the highest intensities usually around the epicentral region and based on subjective information collected from persons who have felt the earthquake at a specific location. Seismic intensity observations in Mexico have been reported in the literature for particular earthquakes (mainly historical events) (e.g., DuBois and Smith, 1980; Suter et al., 1996; Suter, 2015a, 2018, 2019, 2020; Suter and Morelos-Rodríguez, 2023) or in comprehensive earthquake catalogs (Figueroa, 1963, 1986; Suárez, 2021).

Several efforts have been made to develop relationships between seismic intensity and ground motion parameters such as the peak ground acceleration (PGA), peak ground velocity (PGV), peak ground displacement (PGD), seismic magnitude (M), and hypocentral distance (R) among others (Trifunac and Brady, 1975; Murphy and O'Brien, 1977). In the absence of ground motion observations, various

https://doi.org/10.5194/nhess-2024-92
Preprint. Discussion started: 12 June 2024


Natural Hazards and Earth System Sciences Discussions

approaches to model ground motion parameters for different rupture scenarios for historical earthquakes have been explored, including dynamic rupture modeling, kinematic modeling, modeling with ground-motion prediction equations, and stochastic modeling. Various prediction relations from ground motion parameters have been proposed for different regions; for instance, for California (Wald et al., 1999; Atkinson and Sonley, 2000; Atkinson and Kaka, 2007), Taiwan (Wu et al., 2003), Greece (Tselentis and Danciu, 2008), and Turkey (Bilal and Askan, 2014), among other zones. The correlation relationships can be developed in different forms, such as using regional, global, or synthetic data. In this article, we determined conversion relationships between seismic intensities and PGA for 18 historical shallow crustal earthquakes which took place in Mexico with moment magnitudes in the range of 4.5 – 7.5. The seismic events occurred between 1568 and 1989, and seismic intensities were reported in the literature. Since the last $M \geq 6$ event originated in north and central Mexico (we exclude the strike slip regime of northern Baja California Peninsula in this context) took place in 1920, we cannot rely on observed records alone. Therefore, we rely on PGA values generated by synthetic accelerograms derived from the finite-fault stochastic method (Motazedian and Atkinson, 2005). The calculated relationships will be relevant for various purposes ranging from assessment of historical seismicity to several applications in seismic hazard and risk studies from shallow crustal earthquakes in Mexico.

2 Tectonic setting

The epicenters of the studied earthquakes occurred in three tectonic provinces: 1) Basin and Range province (BRP, two events), 2) Sierra Madre Oriental fold-thrust belt (SMOFTB, two events), and 3) the Trans-Mexican Volcanic Belt (TMVB, 14 events) (Fig. 1). The BRP is characterized by the alternance of north-south trending mountains and flat valley floors comprising the province. The 5 March 1887 Bavispe earthquake (M_W = 7.5) occurred in a north-south striking west-dipping normal

https://doi.org/10.5194/nhess-2024-92
Preprint. Discussion started: 12 June 2024


Natural Hazards and Earth System Sciences
Discussions

fault system distributed on the western limit of the Sierra Madre Occidental. This event is considered the largest crustal fault earthquake in Mexico (Suter, 2015b). The rupture has been modeled with a dip angle of 70° and a maximum displacement of 5.2 m and comprises three fault segments (the Pitáycachi, Teras, and Otates segments, respectively) (Suter, 2015b). The second event in the BRP at the Bolaños graben was the 6 November 1774 event (M_W = 5.7) (Suter, 2020). The SMOFTB is the most prominent tectonic characteristic in eastern Mexico and constitutes the continuation to the south of the North American Rocky Mountains. The southern part of the SMOFTB and the northern part of the TMVB are being deformed by mostly north-south-striking extension structures. Two studied earthquakes occurred in this geological structure at a latitude of about 21° in east-central Mexico in a segment 130 km length along the Moctezuma River (Suter, 1987). The TMVB is an active volcanic arc associated with the subduction of oceanic plates along the Pacific margin of Mexico. The TMVB spans over 1200 km, from the Pacific Ocean to the Gulf of Mexico, and is 100 km wide (Ferrari et al., 2012). The western part of the TMVB exhibits three major normal fault systems oriented: NW-SE, NNE-SSW, and WNW-ESE. The central part of the TMVB is characterized by normal faults with a left-lateral strike-slip component orientated east-west. The eastern segment of the central TMVB is dominated by a left-lateral transtensive deformation, whose extension is oriented NW-SE (Ego and Ansan, 2002).

3 Data and methods

We studied ground motion characteristics of 18 historical shallow crustal earthquakes in north and central Mexico with magnitudes in the range of 4.5 – 7.5 (Table 1 and Fig. 1). For this purpose, we used reported seismic intensities (531 MMI observations) in conjunction with synthetic PGA values to derive conversion relationships. Reported MMI values varied from 2 to 11 recorded at hypocentral distances in the range of 8.14 – 1800 km (Fig. 2).

https://doi.org/10.5194/nhess-2024-92
Preprint. Discussion started: 12 June 2024

Natural Hazards and Earth System Sciences
Discussions

3.1 Stochastic finite-fault method

The stochastic strong-ground motion method was proposed by Boore (1983) as a fast and reliable technique for simulating high-frequency characteristics generated by earthquakes. The method has been subsequently improved by incorporating different sources (point or finite-fault models), paths, and site effects (H/V curves or theoretical functions) to calculate synthetic signals (displacement, velocity, or acceleration signals) to be contrasted then with the observed records. We used the stochastic finite-fault ground motion approach developed by Motazedian and Atkinson (2005) as modified by Atkinson and Assatourians (2015) to model ground motions of the selected events. Following that approach, the fault plane is subdivided into a grid of subsources (or subfaults), assigning a stochastic point source to each subfault. Each subfault is activated once with an appropriate delay time. A point source Brune ω^2-source spectrum (Brune, 1970) is generated for each subfault. The point source spectrum is derived by multiplying the source, path, and site spectra in the frequency domain (Boore, 1983; 2003). The acceleration spectrum of a point source is described by the equation

$$Y(M_0, R, f) = A(M_0, f)\,P(R, f)\,S(f) \quad , \tag{1}$$

where $A(M_0, f)$, $S(f)$, and $P(R, f)$ represent the source, site, and path spectra, respectively. M_0 is the seismic moment, R is the hypocentral distance, and f is the frequency. The acceleration spectra after considering the Brune model is (Motazedian and Atkinson, 2005)

$$A(M_0, f)\frac{R_\theta\ VF\,M_0\,H_{ij}(2\pi f)^2}{4\pi\rho\beta^3}G(r)\frac{1}{\left[1+(f/f_c)^2\right]}e^{-\pi f R_{ij}/Q(f)\beta}Z(f)e^{-\pi\kappa f} \quad , \tag{2}$$

where $R_{\theta\varphi}$ is the radiation pattern (0.55), F is the free surface amplification (2.0), V is the partition of

https://doi.org/10.5194/nhess-2024-92
Preprint. Discussion started: 12 June 2024


Natural Hazards and Earth System Sciences
Discussions

energy into two horizontal components (0.7), ρ is the rock density, β is the *S*-wave velocity, f_c is the corner frequency, M_0 is the seismic moment, H_{ij} is a frequency-dependent scaling factor for high-frequencies, $G(R)$ is the geometrical spreading function, $Q(f)$ is the seismic attenuation factor, R_{ij} is the distance from the observation point to the ijth subfault, and $Z(f)$ is a function that describes site amplification. The corner frequency is defined as $f_c = N(t)^{-1/3}\ 4.9 \times 10^6\ \beta\ (\Delta\sigma/M_{0ave})^{1/3}$, where $\Delta\sigma$ is the stress drop, M_{0ave} is the average seismic moment of the fault ($M_{0ave} = M_0/N$, here N is the number of subfaults), and $N(t)$ denotes the cumulative number of all ruptured subfaults at time t. The acceleration spectra ($A(M_0,f)$) is combined with random phases and transferred into the time domain for each point source on the finite-fault plane. The contribution from each subfault is summed up from the entire fault in the time domain with the following equation ($a(t)$)

$$a(t) = \sum_{i=1}^{nl} \sum_{j=1}^{nw} a_{ij}\left(t - \Delta t_{ij} - T_{ij}\right) \quad , \tag{3}$$

where nl is the subfault number along the fault length, nw is the same along the fault width, Δt_{ij} is the relative time delay that the radiated waves from the ijth subfault arrive at the observation point, and T_{ij} is the fraction of rise time. The duration of motion comes from the source duration plus the path duration. The ground motion simulations were performed with the code EXSIM12 (Assatourians and Atkinson, 2012).

3.2 Finite-fault stochastic ground motion simulation input parameters

For the analyzed events, we used moment magnitude. In some cases, it was taken from previous studies (Suter, 2015b; Suárez et al., 2019), but in other cases, it was derived from conversion relationships between m_b and M_W estimated by Scordilis (2006). Seismic velocities and densities at hypocenter

https://doi.org/10.5194/nhess-2024-92
Preprint. Discussion started: 12 June 2024

locations were taken from the 3D elastic model of Mexico derived by Spica et al. (2016). For the case of earthquakes along the TMVB, we used frequency-dependent attenuation models determined by Pérez-Moreno et al. (2021). On the other hand, the seismic attenuation model for the Sonora region (Castro et al., 2008) was used to simulate the March 5, 1887, Bavispe earthquake. Previous studies showed that the spectral decay parameter is in the range of 0.03 – 0.04 sec for crustal earthquakes in Mexico (e.g., Fernandez et al., 2009; Lermo et al., 2016). We calculated fault dimension with the scaling relations for normal-faulting earthquakes following Thingbaijam et al. (2017). Strike and dip angles for the studied events are reported in Table 2. Synthetic slip distributions were generated with the slip spatial random field model proposed by Mai and Beroza (2002) using a von Karman autocorrelation function. We used different stress drop values to perform stochastic ground motion simulations to calculate PGA values (1, 5, 10, and 20 MPa). Site effects were both quantified by generic rock and soil site amplification functions of Boore and Joyner (1997). We used the geometrical spreading and distance-dependent path duration model for eastern North America based on shallow crustal earthquakes proposed by Atkinson and Boore (1995).

3.3 Regression analysis

After obtaining synthetic peak ground acceleration/reported intensity pairs, we fitted the data considering two distinct forms: 1) using the complete dataset and 2) averaging the data by different MMI levels as commonly presented by several authors (e.g., Atkinson and Kaka, 2007; Worden et al., 2012). The latter approach is used to obtain regression results that are stable and well-constrained for each intensity level. The relationship between PGA and intensity pairs is commonly represented by linear models (Wald et al., 1999; Atkinson and Sonley, 2000). As previously reported, inspecting the complete dataset exhibited a two-branched trend (Figs. 3 and 4). In this case, we fitted the data using piecewise linear fitting Python code PWLF (Jekel and Venter, 2019). We adopted an approach similar

https://doi.org/10.5194/nhess-2024-92
Preprint. Discussion started: 12 June 2024

to Atkinson and Kaka (2007) to determine the averaged linear model. We started by finding the mean $\log_{10}$PGA for each MMI level (2 to 10), including in each average the data for MMI 2.0 – 3.75, 3.76 – 4.49, 4.50 – 5.49, 5.50 – 6.49, 6.50 – 7.49, 7.50 – 8.49, 8.50 – 9.49, 9.50 – 10.49, and 10.50 – 11.49. The result followed a linear trend (Figs. 3 and 4). We regressed MMI against the $\log_{10}$ PGA to obtain the bilinear predictive equations of the form (model 1, dark blue lines in Figs. 3 and 4)

$$MMI = c_1 + c_2 \log_{10} PGA \quad \text{for } \log_{10}\text{PGA} \le t_1, \qquad (4)$$
$$MMI = c_3 + c_4 \log_{10} PGA \quad \text{for } \log_{10}\text{PGA} > t_1$$

where c_1 to c_4 are the fitted parameters, and t_1 is intersection of the two lines. On the other hand, the single linear model is here referred to as model 2 (red lines in Figs. 3 and 4). Table 3 summarizes the parameters for each of the regression models. Following Atkinson and Kaka (2007), we applied a correction term to the regressions previously described. This term accounts for magnitude and distance effects and is defined as

$$\Delta_{MMI} = c_5 + c_6 M_W + c_7 \log_{10} R \quad \text{for } \log_{10}\text{PGA} \le t_1, \qquad (5)$$
$$\Delta_{MMI} = c_8 + c_9 M_W + c_{10} \log_{10} R \quad \text{for } \log_{10}\text{PGA} > t_1$$

where M_W is the moment magnitude and R is the hypocentral distance. The coefficients for these regressions are given in Table 4. The improved prediction equations of MMI for PGA are the sum of models 1 to 2 and Eq. (5). In the case of a simple linear model, only one part of Eq. (5) is used.

4 Results

https://doi.org/10.5194/nhess-2024-92
Preprint. Discussion started: 12 June 2024

The regression coefficients and standard errors based on Eqs. (4) and (5) are listed in Tables 3 and 4. Residuals as a function of magnitude and distance are shown in Figs. 5 and 6 for the bilinear and linear models, respectively. We evaluated the variations of residuals versus M_W and hypocentral distance, observing that there is no obvious dependency in the residuals on these parameters. Our results also showed that the residuals are smaller for the linear model by a factor of 8 concerning residuals for the bilinear model. The standard errors of regression equations support this observation; in this case, errors are smaller by factors between 2 and 3 (Table 3). After applying the correction term to the residuals, we observed a slight reduction in the standard errors (Table 4). By comparing results for rock and soil site conditions, our results exhibit similar standard error values (Tables 3 and 4). Our results showed that MMI-PGA relationships derived for stress drop values of 10 and 20 MPa have the lowest standard errors. Figures. 7 to 10 show a comparison of the resulting MMI-PGA models with relations obtained in previous studies for regions with similar tectonic features based on shallow crustal earthquakes. These are discussed in the following section.

5 Discussion and conclusions

We contrasted our results with reported MMI-PGA relations for California ($5.8 < M < 7.3$, Wald et al., 1999; $4.9 < M_W < 7.4$, Atkinson and Sonley, 2000), Central United States ($1.8 < M < 7.1$, Atkinson and Kaka, 2007), Greece ($4 < M < 6.9$, Tselentis and Danciu, 2008), Iran ($5.1 < M_W < 7.3$, Ahmadzadeh et al., 2020), and Türkiye ($5.7 < M_W < 7.4$, Bilal and Askan, 2014) (Figs. 7 to 10). The bilinear models differ significantly at lower PGA values (< 10 cm/s^2). On the other hand, linear models are consistent with most of the relationships reported in previous studies. The observed discrepancies among the MMI-PGA relationships may reflect the differences in input data, especially the macroseismic intensity assignments and the regional tectonic environment.

https://doi.org/10.5194/nhess-2024-92
Preprint. Discussion started: 12 June 2024


Natural Hazards and Earth System Sciences Discussions

The standard errors of our linear models reinforce the observation that the binning procedure proposed by Atkinson and Kaka (2007) provides stable and reliable results. Although the whole data may be considered without averaging, it gives more significant standard errors. In particular, a stress drop value of 10 MPa provides a correlation between PGA and MMI in good agreement with global studies. According to Kanamori and Anderson (1975), a stress drop value of 10 MPa can be considered typical for intraplate earthquakes. On the contrary, Allmann and Shearer (2009) reported a median stress drop of 5.95 ± 1 MPa for intraplate events. If we are to follow this assumption, our regression models determined for a stress drop value of 5 MPa might be the best choice. Our results showed weak dependencies of the residuals on magnitude or distance terms; we also developed refined predictive relationships that include these parameters as independent variables.

In Mexico, few strong-motion recordings of shallow crustal earthquakes have led to uncertainties in the estimation of seismic risk in the region. Estimations of ground motions during these events can be obtained by converting reported MMI to PGA or PGV using conversion relations derived from other regions. This, nevertheless, has not been carried out, mainly because no such conversion relationships were available for Mexico (Córdoba-Montiel et al., 2018). In this sense, we tested our conversion relationships with other PGA estimations, particularly for the 1920 Jalapa earthquake (event 13 in Table 1). Córdoba-Montiel et al. (2018) determined a PGA for the Jalapa City (MMI = 9, with $\Delta\sigma$ = 5 and 10 MPa) of 100 - 250 cm/s^2. Our estimates of PGA are consistent with their results for the same stress drops (176 < PGA < 300 cm/s^2). Our conversion relations are the first MMI-PGA relations proposed for north and Central Mexico. Overall, our results showed that the stochastic ground motion simulation method is a valid methodology to determine MMI-PGA relations consistent with those derived with peak ground motion observations, being a suitable option to add to the study the effects of historical earthquakes with MMI observations available. The proposed methodology can be improved by

https://doi.org/10.5194/nhess-2024-92
Preprint. Discussion started: 12 June 2024

including precise site effect estimations (e.g., horizontal-to-vertical spectral ratio, H/V) instead of considering generic site effects. The predictive equations herein proposed can also be used to produce intensity maps for shallow crustal earthquakes in Mexico.

Author contributions. QRP and FRZ designed the framework of the manuscript. QRP performed ground motions simulations and regression analysis. All the authors discussed the results and wrote the paper.

Code availability. Bilinear regression analysis was performed with the PWLF code (https://github.com/cjekel/piecewise_linear_fit_py, Jekel and Venter, 2019). We used the software EXSIM12 to simulate ground motions (https://github.com/GFZ-Centre-for-Early-Warning/exsim, Assatourians and Atkinson, 2012).

Competing interests. The authors declare no competing interests.

Financial support. QRP was supported by the Mexican National Council for the Humanities, Science, and Technology (CONAHCYT) (Catedras program - project 1126).

References

Ahmadzadeh, S., Doloei, G.J., Zafarani, H.: Ground Motion to Intensity Conversion Equations for Iran, Pure Appl. Geophys., 177, 5435-5449, https://doi.org/10.1007/s00024-020-02586-x, 2020.

Allmann, B.P., Shearer, P.M.: Global variations of stress drop for moderate to large earthquakes, J. Geophys. Res., 114, B01310, https://doi.org/10.1029/2008JB005821, 2009.

https://doi.org/10.5194/nhess-2024-92
Preprint. Discussion started: 12 June 2024

Assatourians, K., Atkinson, G.M.: EXSIM12: A stochastic finite - fault computer program in FORTRAN, https://github.com/GFZ-Centre-for-Early-Warning/exsim, 2012.

Atkinson, G.M., Boore, D.M.: Ground motion relations for eastern North America, Bull. Seismol. Soc. Am., 85, 17-30, https://doi.org/10.1785/BSSA0850010017, 1995.

Atkinson, G.M., Sonley, E.: Empirical relationships between modified Mercalli intensity and response spectra, Bull. Seismol. Soc. Am., 90, 537-544, https://doi.org/10.1785/0119990118, 2000.

Atkinson, G.M., Kaka, S.I.: Relationships between felt intensity and instrumental ground motion in the central United States and California, Bull. Seismol. Soc. Am., 97, 497-510, https://doi.org/10.1785/0120060154, 2007.

Atkinson, G.M., Assatourians, K.: Implementation and validation of EXSIM (a stochastic finite-fault ground-motion simulation algorithm) on the SCEC broadband platform, Seismol. Res. Lett., 86, 48-60, https://doi.org/10.1785/0220140097, 2015.

Bilal, M., Askan, A.: Relationships between felt intensity and recorded ground-motion parameters for Turkey, Bull. Seismol. Soc. Am., 104, 484-496, https://doi.org/10.1785/0120130093, 2014.

Boore, D.M.: Stochastic simulation of high-frequency ground motions based on seismological models of the radiated spectra, Bull. Seismol. Soc. Am., 73, 1865-1894, https://doi.org/10.1785/BSSA07306A1865, 1983.

https://doi.org/10.5194/nhess-2024-92
Preprint. Discussion started: 12 June 2024

Boore, D.M., Joyner, W.B.: Site amplifications for generic rock sites, Bull. Seismol. Soc. Am., 87, 327-341, https://doi.org/10.1785/BSSA0870020327, 1997.

Boore, D.M.: Simulation of ground motion using the stochastic method, Pure Appl. Geophys., 160, 635-676, https://doi.org/10.1007/PL00012553, 2003.

Brune, J.N.: Tectonic stress and the spectra of seismic shear waves from earthquakes, J. Geophys. Res., 75, 4997-5009, https://doi.org/10.1029/JB075i026p04997, 1970.

Castro, R.R., Condori, C., Romero, O., Jacques, C., Suter, M.: Seismic attenuation in Northeastern Sonora, Mexico, Bull. Seismol. Soc. Am., 98, 722-732, https://doi.org/10.1785/0120070062, 2008.

Córdoba-Montiel, F., Singh, S.K., Iglesias, A., Pérez-Campos, X., Sieron, K.: Estimation of ground motion in Xalapa, Veracruz, Mexico during the 1920 (M ~ 6.4) crustal earthquake, and some significant intraslab earthquakes of the last century, Geofis. Int., 57, 89-106, https://doi.org/10.22201/igeof.00167169p.2018.57.2.2039, 2018.

DuBois, S.M., Smith, A.W.: The 1887 earthquake in San Bernardino valley, Sonora. State of Arizona, Bureau of Geology and Mineral Technology, Special Paper 3, 112, 1980.

Ego, F., Ansan, V.: Why is the Central Trans-Mexican Volcanic Belt (102°-99°W) in transtensive deformation?, Tectonophysics, 359, 189-208, https://doi.org/10.1016/S0040-1951(02)00511-5, 2002.

https://doi.org/10.5194/nhess-2024-92
Preprint. Discussion started: 12 June 2024

Ferrari, L., Orozco-Esquivel, T., Manea, V., Manea, M.: The dynamic history of the Trans-Mexican Volcanic Belt and the Mexico subduction zone, Tectonophysics, 522, 122-149, https://doi.org/10.1016/j.tecto.2011.09.018, 2012.

Fernández, A.I., Castro, R.R., Huerta, C.I.: The spectral decay parameter kappa in Northeastern Sonora, Mexico, Bull. Seismol. Soc. Am., 100, 196-206, https://doi.org/10.1785/0120090049, 2010.

Figueroa, J.A.: Isosistas de macrosismos Mexicanos, Reporte, Instituto Ingeneria, Universidad National Autonoma de Mexico, Instituto de Ingeniería, 22 pp., 1963.

Figueroa, J.A.: Isosistas de grandes temblores ocurridos en la República Mexicana, Reporte, Instituto de Ingeniería, Universidad Nacional Autonoma de Mexico, Mexico, 57 pp., 1986.

Jekel, C.F., Venter, G.: pwlf: A Python library for fitting 1D continuous piecewise linear functions, https://doi.org/10.13140/RG.2.2.28530.56007, 2019.

Kanamori, H., Anderson, D.L.: Theoretical basis of some empirical relations in Seismology, Bull. Seismol. Soc. Am., 65, 1073-1095, https://doi.org/10.1785/BSSA0650051073, 1975.

Lermo, J., Santoyo, M.A., Jaimes, M.A., Antayhua, Y., Chavacán, M.: Local earthquakes of the Mexico basin in Mexico City: κ, Q, source spectra, and stress drop, Bull. Seismol. Soc. Am., 106, 1423-1437, https://doi.org/10.1785/0120150189, 2016.

Mai, P.M., Beroza, G.C.: A spatial random-field model to characterize complexity in earthquake slip, J.

https://doi.org/10.5194/nhess-2024-92
Preprint. Discussion started: 12 June 2024

Geoph. Res., 107, 2308, https://doi.org/10.1029/2001JB000588, 2002.

Mallet, R.: Great Neapolitan Earthquake of 1857. The first principles of observational seismology, Chapman and Hall, London, 1862.

Motazedian, D., Atkinson, G.M.: Stochastic finite-fault modeling based on a dynamic corner frequency, Bull. Seismol. Soc. Am., 95, 995-1010, https://doi.org/10.1785/0120030207, 2005.

Murphy, J.R., O'Brien, L.J.: The correlation of peak ground acceleration amplitude with seismic intensity and other physical parameters, Bull. Seismol. Soc. Am., 67, 877-915, https://doi.org/10.1785/BSSA0670030877, 1977.

Pérez-Moreno, F., Rodríguez-Pérez, Q., Zúñiga, F.R., Horta-Rangel, J., Arroyo, M., Pérez-Rea, M.L., Morales-Chico, R.: Coda waves attenuation in the Trans-Mexican Volcanic Belt considering local seismicity, J. Seismol., 25, 461-475, https://doi.org/10.1007/s10950-021-09987-y, 2021.

Scordilis, E.M.: Empirical global relations converting M_S and m_b to moment magnitude, J. Seismol., 10, 225-236, https://doi.org/10.1007/s10950-006-9012-4, 2006.

Suárez, G., Caballero-Jiménez, G.V., Novelo-Casanova, D.A.: Active crustal deformation in the Trans-Mexican Volcanic Belt as evidenced by historical earthquakes during the last 450 years, Tectonics, 38, 3544-3562, https://doi.org/10.1029/2019TC005601, 2019.

Spica, Z., Perton, M., Calò, M., Legrand, D., Córdoba-Montiel, F., Iglesias, A.: 3-D shear wave

https://doi.org/10.5194/nhess-2024-92
Preprint. Discussion started: 12 June 2024

velocity model of Mexico and South US: bridging seismic networks with ambient noise cross-correlations (C1) and correlation of coda of correlations (C3), Geophys. J. Int., 206, 1795-1813, https://doi.org/10.1093/gji/ggw240, 2016.

Suter, M.: Structural traverse across the Sierra Madre Oriental fold-thrust belt in east-central Mexico, GSA Bulletin, 98, 249-264, https://doi.org/10.1130/0016-7606(1987)98<249:STATSM>2.0.CO;2, 1987.

Suter, M., Carrillo-Martínez, M., Quintero-Legorreta, O.: Macroseismic study of shallow earthquakes in the Central and Eastern parts of the Trans-Mexican Volcanic Belt, Mexico, Bull. Seismol. Soc. Am. 86, 1952-1963, https://doi.org/10.1785/BSSA0860061952, 1996.

Suter, M.: The A.D. 1567 MW 7.2 Ameca, Jalisco, earthquake (Western Trans-Mexican Volcanic Belt): surface rupture parameters, seismological effects, and macroseismic intensities from historical source, Bull. Seismol. Soc. Am., 105, 646-656, https://doi.org/10.1785/0120140163, 2015a.

Suter, M.: Rupture of the Pitáycachi Fault in the 1887 M_W 7.5 Sonora, Mexico earthquake (southern basin-and-range province): rupture kinematics and epicenter inferred from rupture branching patterns, J. Geophys. Res., 120, 617-641, https://doi.org/10.1002/2014JB011244, 2015b.

Suter, M.: The 2 October 1847 MI 5.7 Chapala graben triggered earthquake (Trans-Mexican Volcanic Belt, West-Central Mexico): Macroseismic observations and hazard implications, Seismol. Res. Lett., 89, 35-46, https://doi.org/10.1785/0220170101, 2018.

https://doi.org/10.5194/nhess-2024-92
Preprint. Discussion started: 12 June 2024

Suter, M.: Macroseismic study of the devastating 22-23 October 1749 earthquake doublet in the Northern Colima graben (Trans-Mexican Volcanic Belt, Western Mexico), Seismol. Res. Lett., 90, 2304-2317, https://doi.org/10.1785/0220190162, 2019.

Suter, M.: The 6 November 1774 MI 6 Bolaños graben earthquake (Southern basin and range province, West-Central Mexico): Macroseismic observations and neotectonic implications, Bull. Seismol. Soc. Am., 91, 2473-2486, https://doi.org/10.1785/BSSA0860061952, 2020.

Suter, M., Morelos-Rodríguez, L.: Seismotectonics of the Querétaro region (Central Mexico) and the 1934 M_I 4.8 earthquake North of Celaya, Seismol. Res. Lett., 95, 820-833, https://doi.org/10.1785/0220230256, 2023.

Suárez, G.: Historical earthquakes catalog of Mexico, http://www.sismoshistoricos.org, 2021.

Thingbaijam, K.K.S., Mai, P.M., Goda, K.: New empirical earthquake source-scaling laws, Bull. Seismol. Soc. Am., 107, 2225-2246, https://doi.org/10.1785/0120170017, 2017.

Trifunac, M.D., Brady, A.G.: On the correlation of seismic intensity scales with the peaks of recorded strong ground motion, Bull. Seismol. Soc. Am., 65, 139-162, https://doi.org/10.1785/BSSA0650010139, 1975.

Tselentis, G.A., Danciu, L.: Empirical relationships between modified Mercalli intensity and engineering ground-motion parameters in Greece, Bull. Seismol. Soc. Am., 98, 1863-1875, https://doi.org/10.1785/0120070172, 2008.

https://doi.org/10.5194/nhess-2024-92
Preprint. Discussion started: 12 June 2024

Wald, D.J., Quitoriano, V., Heaton, T.H., Kanamori, H.: Relationships between peak ground acceleration, peak ground velocity, and modified Mercalli intensity in California, Earthq. Spectra, 15, 557-564, https://doi.org/10.1193/1.1586058, 1999.

Wood, H.O., Neumann, F.: Modified Mercalli intensity scale of 1931, Bull. Seismol. Soc. Am., 21, 277-283, https://doi.org/10.1785/BSSA0210040277, 1931.

Wu, Y-H., Teng, T-L., Shin, T-C., Hsiao. N-C.: Relationship between peak ground acceleration, peak ground velocity, and intensity in Taiwan, Bull. Seismol. Soc. Am., 93, 386-396, https://doi.org/10.1785/0120020097, 2003.

Worden, C.B., Gerstenberger, M.C., Rhoades, D.A., Wald, D.J.: Probabilistic relationships between ground-motion parameters and modified Mercalli intensity in California, Bull. Seismol. Soc. Am., 102, 204-221, https://doi.org/10.1785/0120110156, 2012.

https://doi.org/10.5194/nhess-2024-92
Preprint. Discussion started: 12 June 2024

Natural Hazards and Earth System Sciences
Discussions

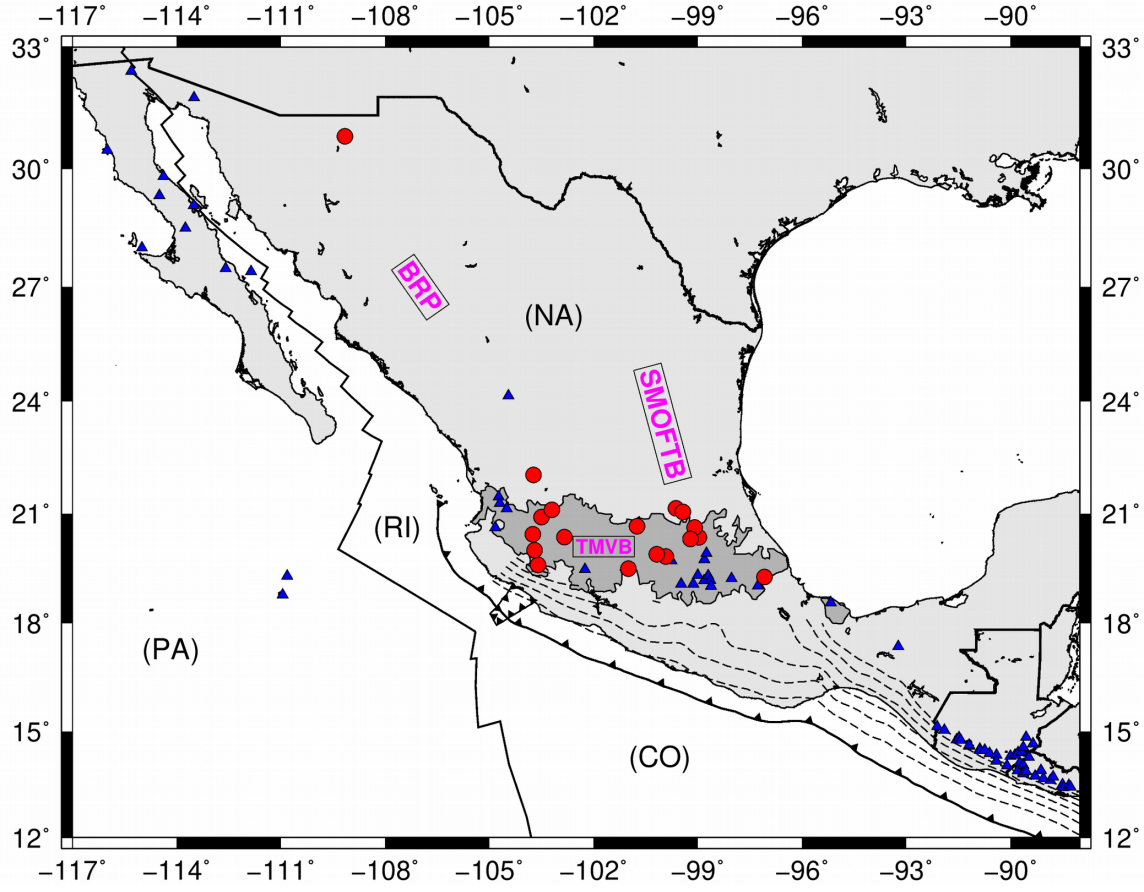

Figure 1. Epicenter locations of the studied earthquakes (red dots). Blue triangles are volcanoes. NA, RI, CO, and PA are the North America, Rivera, Cocos and Pacific plates. BRP is the Basin and Range province, SMOFTB is the Sierra Madre Oriental fold-thrust belt, and TMVB is the Trans-Mexican Volcanic Belt.

https://doi.org/10.5194/nhess-2024-92
Preprint. Discussion started: 12 June 2024

Natural Hazards and Earth System Sciences
Discussions

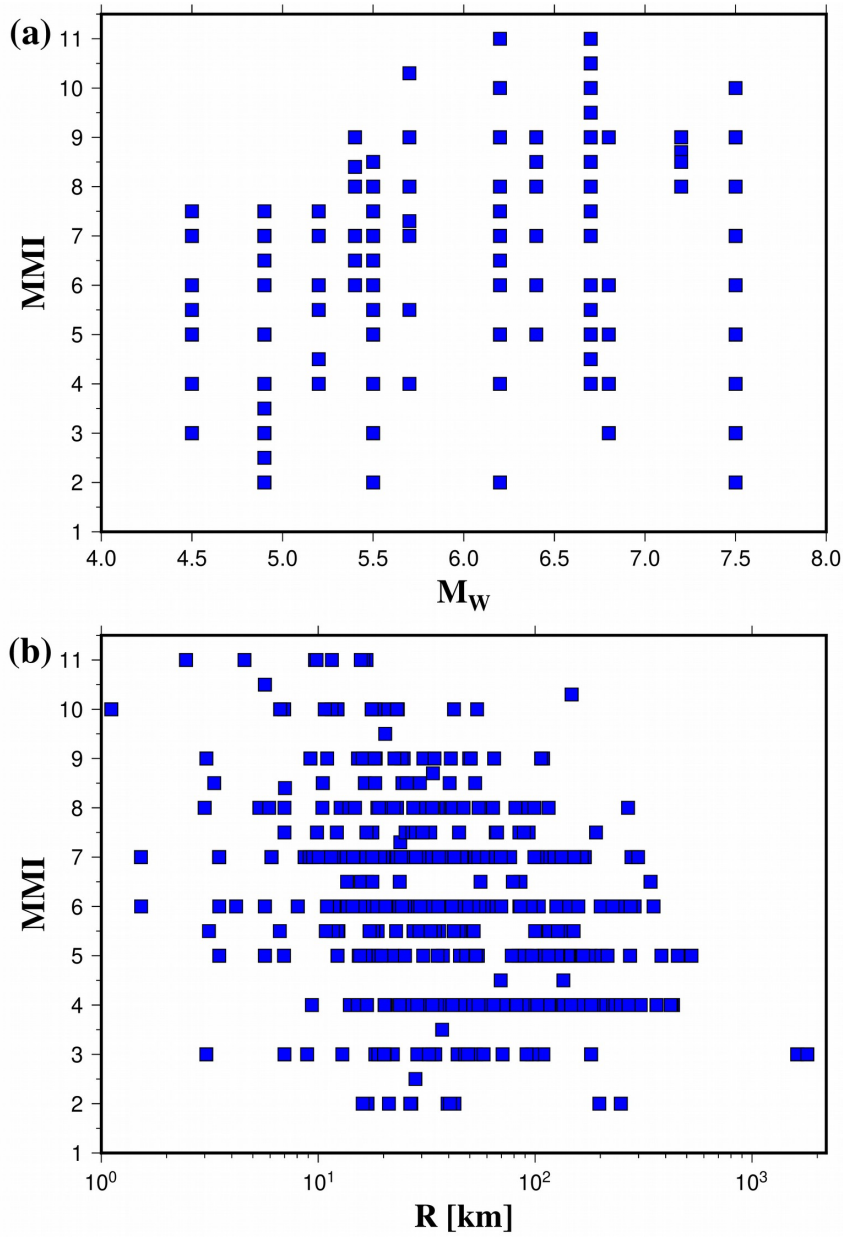

Figure 2. (a) Modified Mercalli intensity (MMI) versus moment magnitude (M_W) of historical shallow earthquakes in Mexico. **(b)** MMI versus hypocentral distance (R) of the studied earthquakes.

https://doi.org/10.5194/nhess-2024-92
Preprint. Discussion started: 12 June 2024

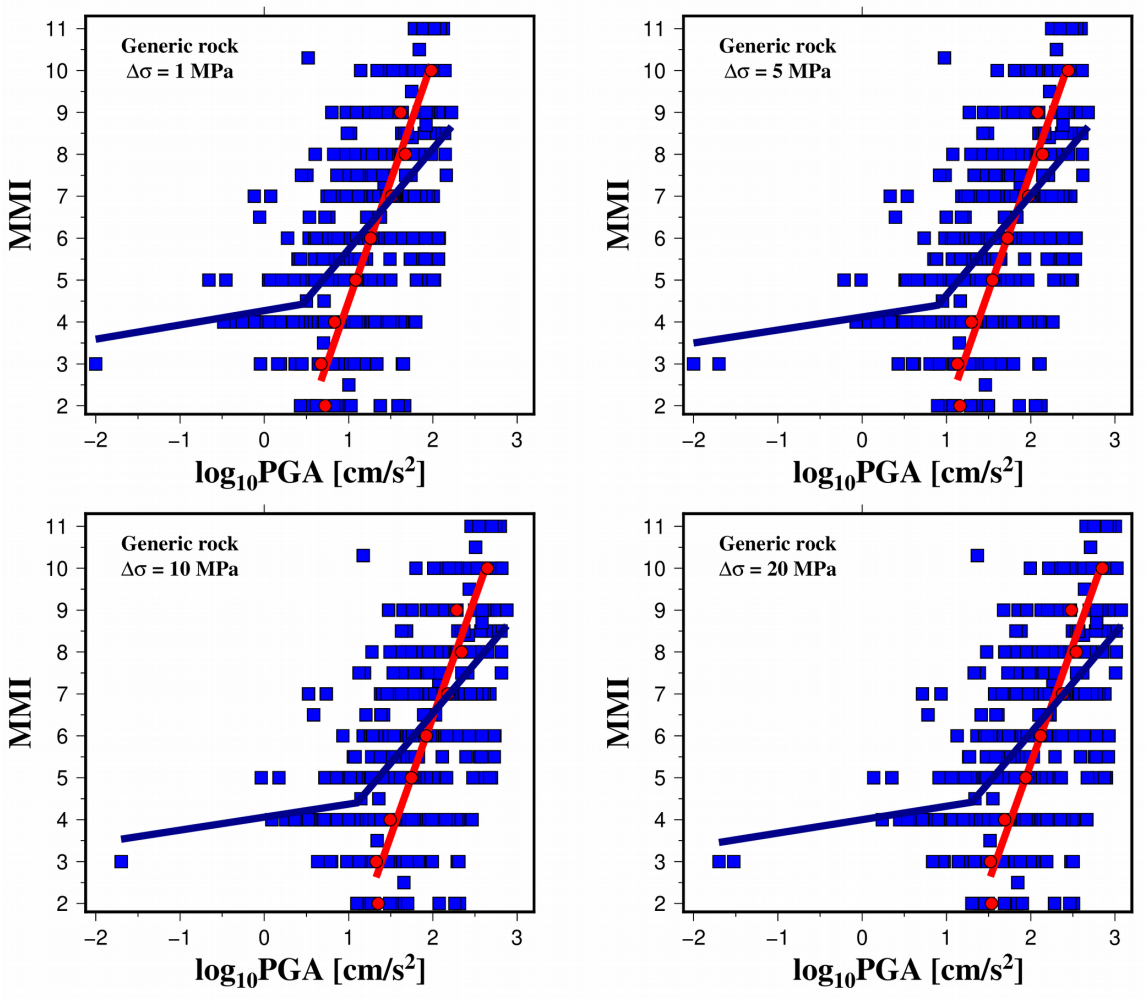

Figure 3. Synthetic peak ground acceleration/reported intensity pairs considering generic rock site and different stress drop conditions (Δσ = 1, 5, 10, and 20 MPa) (blue squares). Red circles represent mean $\log_{10}$ PGA values for each MMI level. Predictive relationships derived in this study: bilinear fit (dark blue lines) and averaged data linear fit (red line).

https://doi.org/10.5194/nhess-2024-92
Preprint. Discussion started: 12 June 2024

Natural Hazards and Earth System Sciences
Discussions

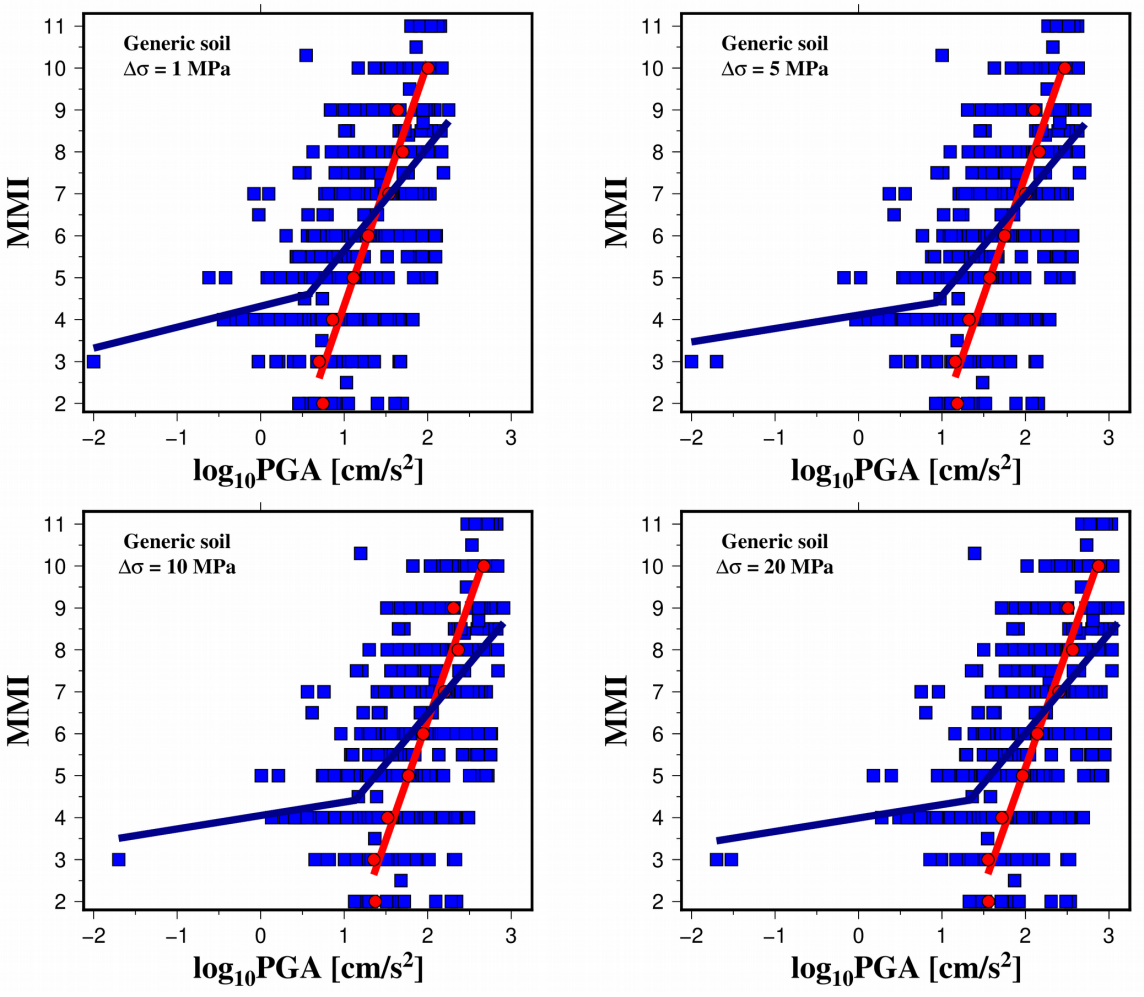

Figure 4. Synthetic peak ground acceleration/reported intensity pairs considering generic soil site and different stress drop conditions ($\Delta\sigma$ = 1, 5, 10, and 20 MPa) (blue squares). Red circles represent mean $\log_{10}$ PGA values for each MMI level. Predictive relationships derived in this study: bilinear fit (dark blue lines) and averaged data linear fit (red line).

https://doi.org/10.5194/nhess-2024-92
Preprint. Discussion started: 12 June 2024

Natural Hazards and Earth System Sciences
Discussions

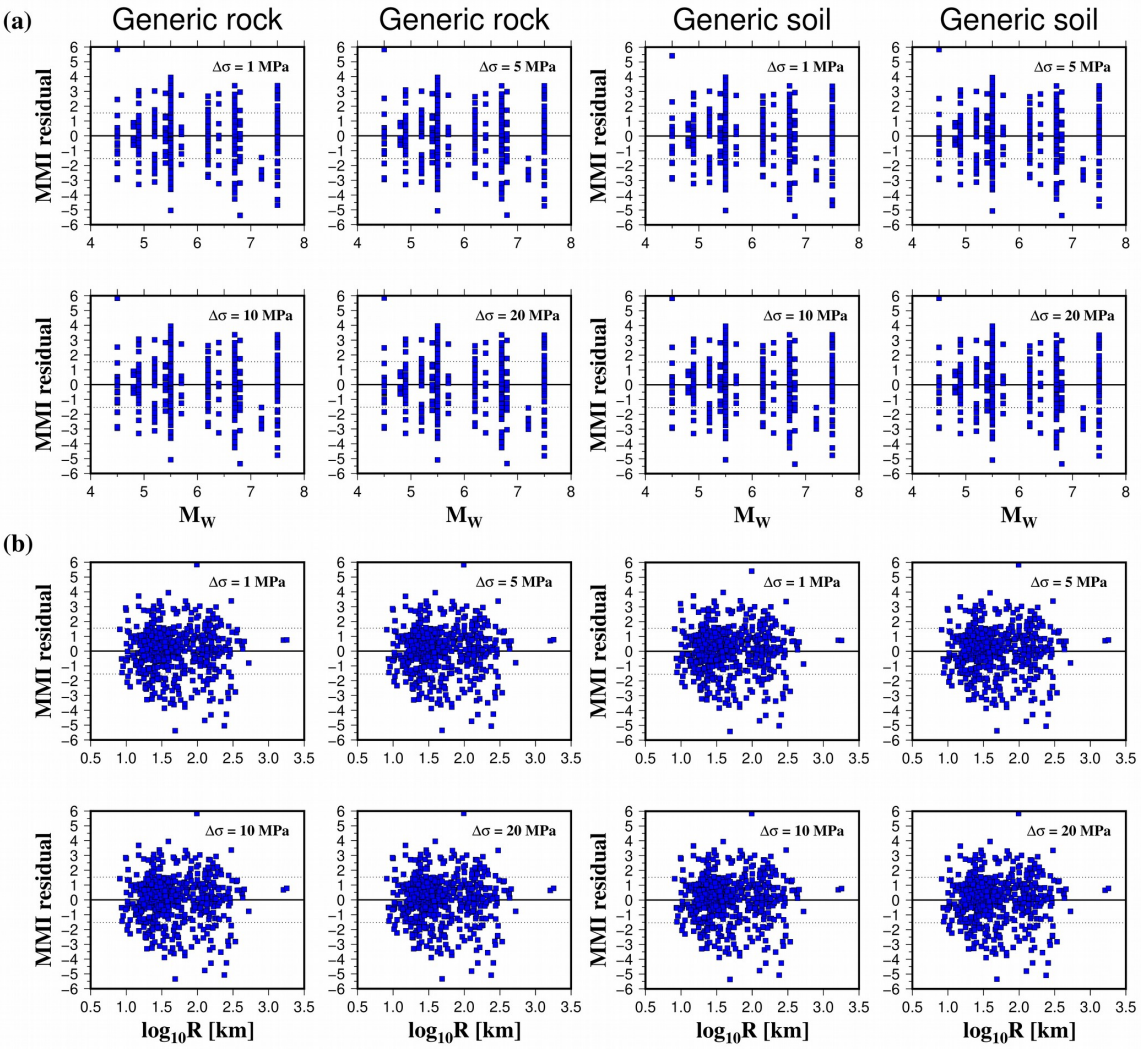

Figure 5. Residuals (observed MMI minus predicted MMI) for MMI predicted from PGA obtained from the bilinear model as a function of earthquake magnitude **(a)** and the log of hypocentral distance **(b)**.

https://doi.org/10.5194/nhess-2024-92
Preprint. Discussion started: 12 June 2024

Natural Hazards and Earth System Sciences
Discussions

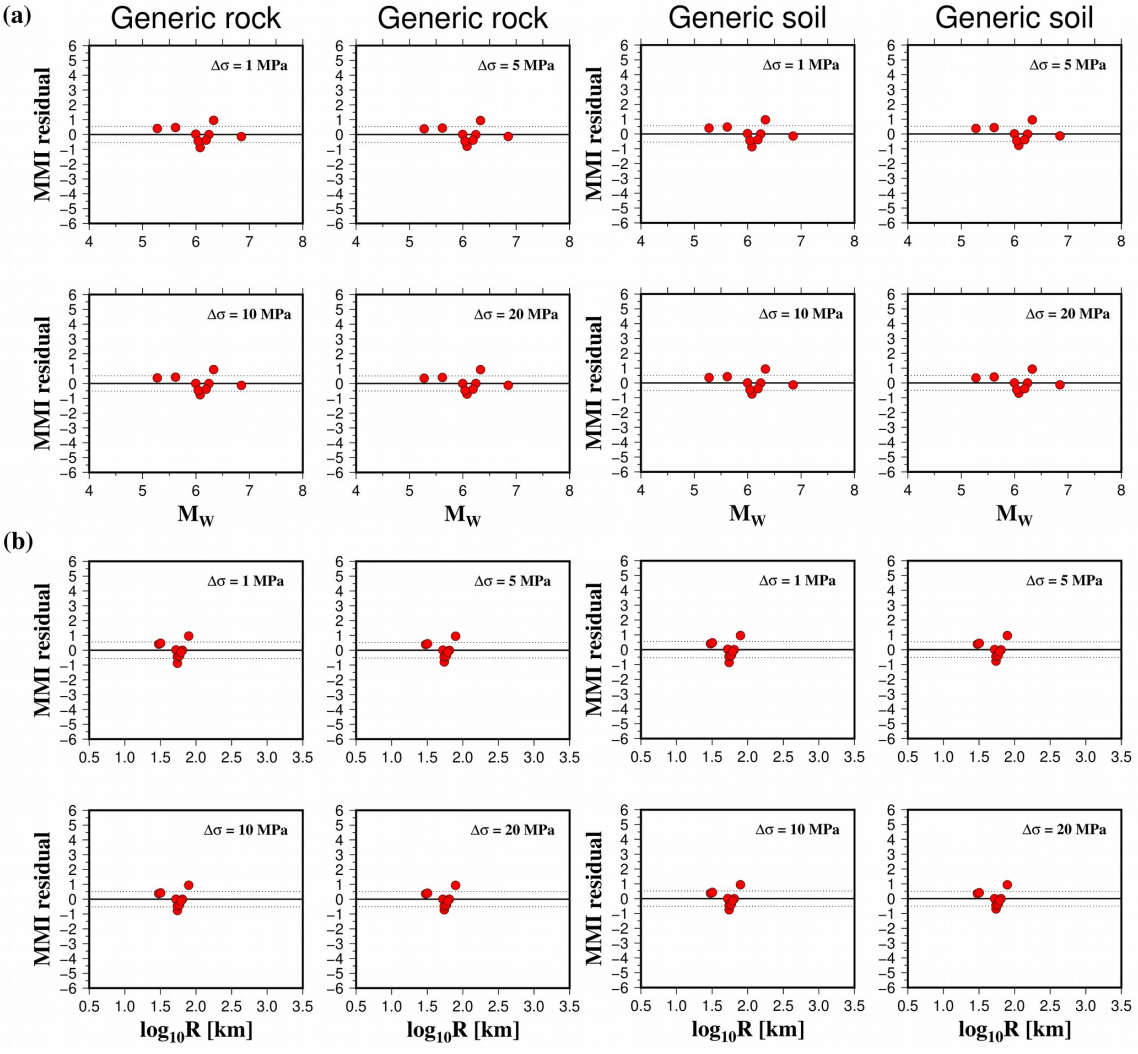

Figure 6. Residuals (observed MMI minus predicted MMI) for MMI predicted from PGA obtained from the averaged data linear fit as a function of earthquake magnitude **(a)** and the log of hypocentral distance **(b)**.

https://doi.org/10.5194/nhess-2024-92
Preprint. Discussion started: 12 June 2024

Natural Hazards and Earth System Sciences
Discussions

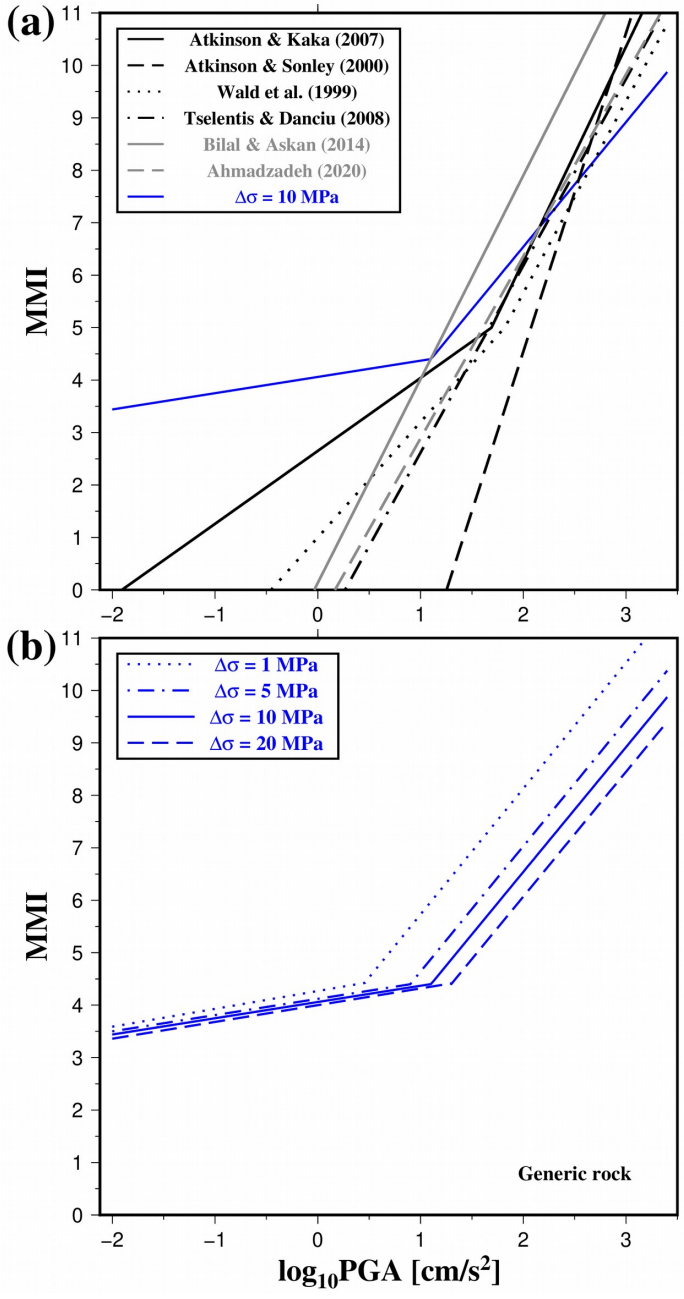

Figure 7. (a) Comparison of the obtained MMI-PGA relationships (blue lines) considering generic rock site conditions with previous studies. **(b)** The lower panel shows results for different stress drop values.

https://doi.org/10.5194/nhess-2024-92
Preprint. Discussion started: 12 June 2024

Natural Hazards and Earth System Sciences
Discussions

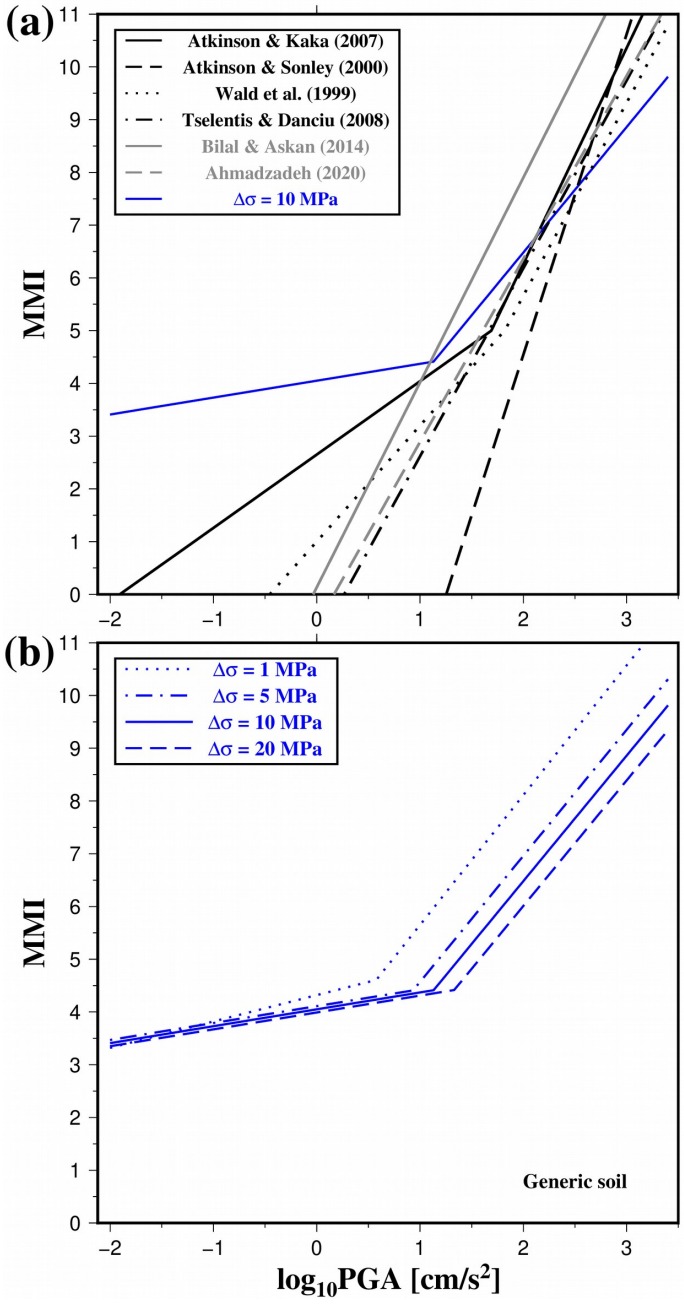

Figure 8. (a) Comparison of the obtained MMI-PGA relationships (blue lines) considering generic soil site conditions with previous studies. **(b)** The lower panel shows results for different stress drop values.

https://doi.org/10.5194/nhess-2024-92
Preprint. Discussion started: 12 June 2024

Natural Hazards and Earth System Sciences
Discussions

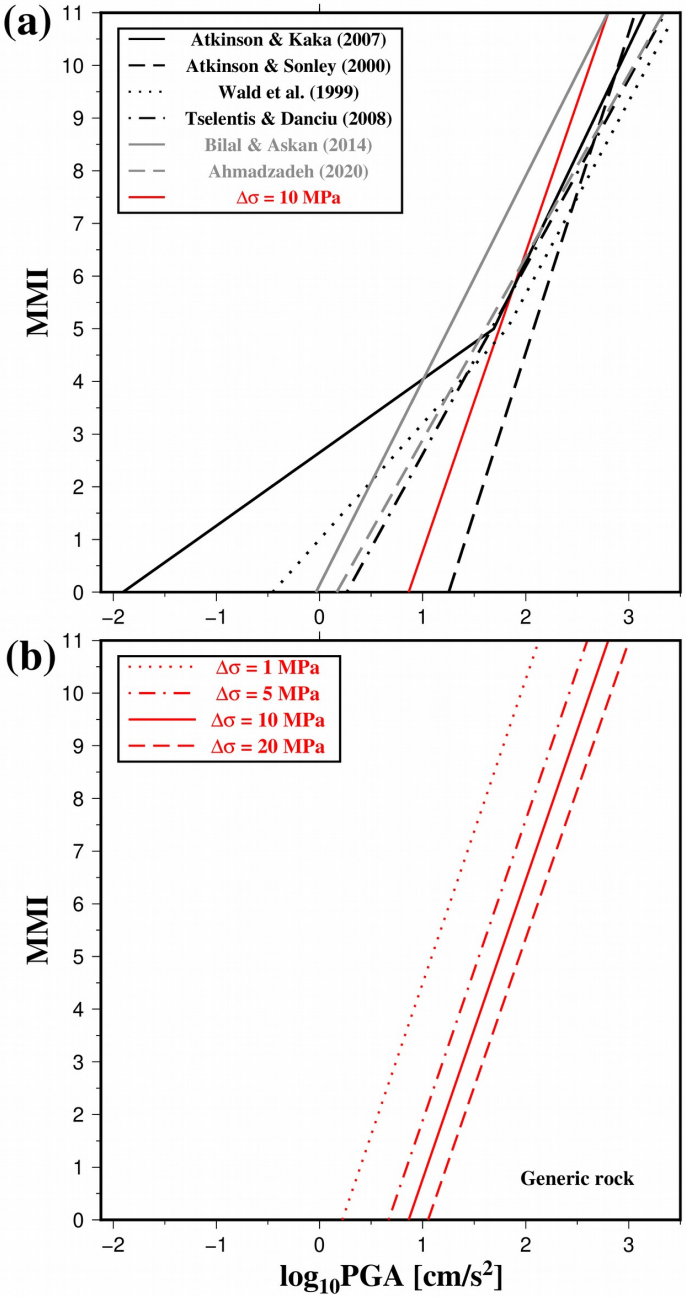

Figure 9. (a) Comparison of the obtained MMI-PGA relationships (red lines) considering generic rock site conditions for the averaged data with previous studies. **(b)** The lower panel shows results for different stress drop values.

https://doi.org/10.5194/nhess-2024-92
Preprint. Discussion started: 12 June 2024

Natural Hazards and Earth System Sciences
Discussions

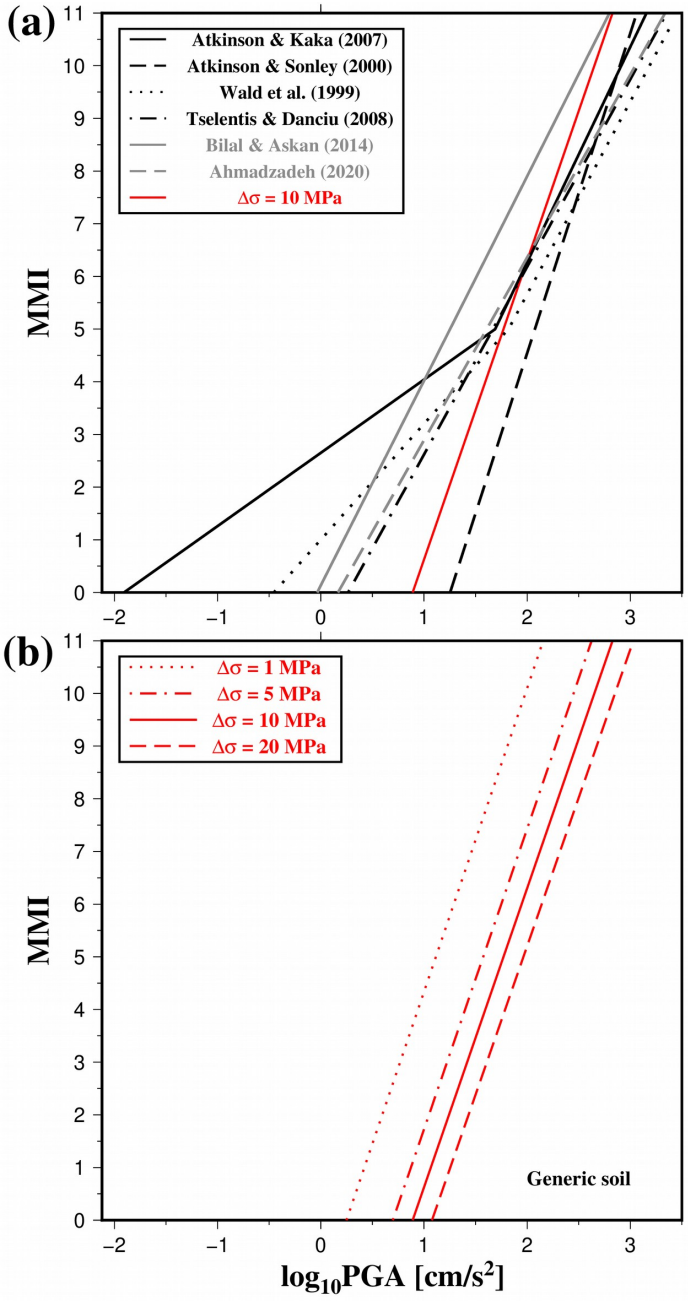

Figure 10. (a) Comparison of the obtained MMI-PGA relationships (red lines) considering generic soil site conditions for the averaged data with previous studies. **(b)** The lower panel shows results for different stress drop values.

https://doi.org/10.5194/nhess-2024-92
Preprint. Discussion started: 12 June 2024

Natural Hazards and Earth System Sciences
Discussions

Table 1. Studied earthquakes (M_W – moment magnitude)

Event	Date dd/mm/yyyy	Longitude (°)	Latitude (°)	Depth [km]	M_W	Seismic Intensity Data
1	27/12/1568	-103.74	20.43	15	7.2	Suter (2015)
2	15/04/1611	-103.60	19.60	15	6.4	Suarez (2021)
3	23/10/1749	-103.70	20.00	15	6.4	Suter (2019)
4	12/12/1771	-103.50	20.90	10	5.5	Suarez (2021)
5	06/11/1774	-103.73	22.04	10	5.7	Suter (2020)
6	02/10/1847	-102.84	20.36	10	5.4	Suter (2018)
7	19/06/1858	-101.00	19.50	15	7.5	Suarez (2021)
8	11/02/1875	-103.20	21.10	15	6.8	Suarez (2021)
9	05/03/1887	-109.16	30.81	18	7.5	DuBois and Smith (1980)
10	26/11/1887	-99.63	21.14	10	5.5	Suter et al. (1996)
11	19/12/1912	-99.92	19.83	15	6.7	Suter et al. (1996)
12	14/07/1934	-100.75	20.65	10	4.8	Suter and Morelos-Rodriguez (2023)
13	04/01/1920	-97.08	19.27	12	6.2	Suter et al. (1996)
14	11/03/1950	-98.97	20.35	10	5.2	Suter et al. (1996)
15	25/03/1976	-99.09	20.62	10	5.5	Suter et al. (1996)
16	22/02/1979	-100.18	19.89	8	5.5	Suter et al. (1996)
17	27/01/1987	-99.21	20.31	10	4.5	Suter et al. (1996)
18	10/09/1989	-99.43	21.04	10	4.9	Suter et al. (1996)

https://doi.org/10.5194/nhess-2024-92
Preprint. Discussion started: 12 June 2024

Natural Hazards and Earth System Sciences
Discussions

Table 2. Input parameters for finite-fault stochastic ground motion simulations ($Q(f)$ – attenuation model, κ – spectral decay parameter, β – *S*-wave velocity, ρ – density, L – fault length, ΔL – subfault length, W – fault width, ΔW – subfault width, φ – strike, θ – dip, $\Delta\sigma$ – stress drop)

N	$Q(f)$	κ	β [km/s]	ρ [kg/m³]	L [km]	ΔL [km]	W [km]	ΔW [km]	φ [°]	θ [°]	$\Delta\sigma$ [MPa]	Site conditions
1	$113f^{0.98}$	0.03	3.30	2360	60	6	30	6	150	50	1 5 10 20	generic rock/soil
2	$113f^{0.98}$	0.03	3.58	2416	24	3	16	4	5	60	1 5 10 20	generic rock/soil
3	$113f^{0.98}$	0.03	3.31	2362	24	3	16	4	10	70	1 5 10 20	generic rock/soil
4	$113f^{0.98}$	0.03	3.75	2450	9	3	9	3	200	50	1 5 10 20	generic rock/soil
5	$113f^{0.98}$	0.03	3.59	2418	10	2	10	2	15	60	1 5 10 20	generic rock/soil
6	$113f^{0.98}$	0.03	3.73	2446	8	2	8	2	87	55	1 5 10 20	generic rock/soil
7	$142f^{1.20}$	0.03	3.27	2354	80	8	40	8	265	70	1 5 10 20	generic rock/soil
8	$113f^{0.98}$	0.03	3.48	2396	40	4	20	4	165	50	1 5 10 20	generic rock/soil
9	$84f^{0.90}$	0.04	3.54	2408	80	8	40	8	12	70	1 5 10 20	generic rock/soil
10	$107f^{0.98}$	0.04	3.50	2400	9	3	9	3	10	50	1 5 10 20	generic rock/soil
11	$107f^{0.98}$	0.04	3.45	2390	30	3	20	4	296	60	1 5 10 20	generic rock/soil
12	$107f^{0.98}$	0.04	3.41	2382	4	1	5	1	5	65	1 5 10 20	generic rock/soil
13	$186f^{0.86}$	0.03	3.68	2436	18	3	15	3	72	50	1 5 10 20	generic rock/soil
14	$107f^{0.98}$	0.04	3.47	2394	6	1	7	1	270	50	1 5 10 20	generic rock/soil
15	$107f^{0.98}$	0.04	3.39	2378	9	3	9	3	270	50	1 5 10 20	generic rock/soil
16	$107f^{0.98}$	0.04	3.45	2390	9	3	9	3	280	66	1 5 10 20	generic rock/soil
17	$107f^{0.98}$	0.04	3.58	2416	3	1	4	1	270	50	1 5 10 20	generic rock/soil
18	$107f^{0.98}$	0.04	3.36	2372	5	1	6	1	10	50	1 5 10 20	generic rock/soil

https://doi.org/10.5194/nhess-2024-92
Preprint. Discussion started: 12 June 2024

Natural Hazards and Earth System Sciences
Discussions

Table 3. Results of regressions (GR – generic rock; GS – generic soil; Δσ – stress drop; c_1, c_2, c_3, and c_4 – regression coefficients; t_1 – intersection of the bilinear model; σ_{12} and σ_{34} – standard errors of equations)

Model	Site	Δσ [MPa]	c_1	c_2	c_3	c_4	t_1	σ_{12}	σ_{34}
1	GR	1	4.27	0.34	3.33	2.40	0.46	0.98	1.61
		5	4.12	0.31	2.25	2.39	0.90	0.92	1.61
		10	4.06	0.31	1.78	2.38	1.10	0.92	1.61
		20	4.00	0.32	1.31	2.38	1.30	0.86	1.61
1	GS	1	4.32	0.50	3.19	2.46	0.58	1.22	1.60
		5	4.11	0.32	2.18	2.39	0.93	0.92	1.61
		10	4.05	0.32	1.72	2.38	1.13	0.91	1.62
		20	3.99	0.32	1.25	2.38	1.33	0.91	1.61
2	GR	1	-1.28	5.77				0.55	
		5	-3.83	5.71				0.53	
		10	-4.91	5.68				0.52	
		20	-5.94	5.64				0.51	
2	GS	1	-1.44	5.77				0.55	
		5	-3.99	5.71				0.53	
		10	-5.06	5.68				0.51	
		20	-6.08	5.64				0.50	

https://doi.org/10.5194/nhess-2024-92
Preprint. Discussion started: 12 June 2024

Natural Hazards and Earth System Sciences
Discussions

Table 4. Results of regressions for the magnitude and distance residual correction term (Δ_{MMI}) (GR – generic rock; GS – generic soil; $\Delta\sigma$ – stress drop; c_5, c_6, c_7, c_8, c_9, and c_{10} – regression coefficients; t_1 – intersection of the bilinear model; σ_{12} and σ_{34} – standard errors of equations)

Model	Site	$\Delta\sigma$ [MPa]	c_5	c_6	c_7	c_8	c_9	c_{10}	t_1	σ_{12}	σ_{34}
1	GR	1	2.46	-0.54	0.15	-0.17	0.06	-0.10	0.46	0.96	1.61
		5	1.87	-0.40	0.07	-0.17	0.05	-0.09	0.90	0.91	1.61
		10	1.88	-0.40	0.07	-0.17	0.06	-0.09	1.10	0.91	1.61
		20	2.25	-0.43	-0.08	-0.23	0.06	-0.08	1.30	0.84	1.61
1	GS	1	3.31	-0.64	-0.06	-0.29	0.08	-0.10	0.58	1.19	1.60
		5	1.89	-0.40	0.06	-0.17	0.05	-0.09	0.93	0.91	1.61
		10	1.95	-0.41	0.07	-0.18	0.06	-0.09	1.13	0.90	1.61
		20	1.96	-0.41	0.06	-0.19	0.06	-0.09	1.33	0.90	1.61
2	GR	1	1.62	-0.47	0.70					0.53	
		5	1.46	-0.45	0.75					0.51	
		10	1.40	-0.45	0.77					0.50	
		20	1.29	-0.44	0.80					0.49	
2	GS	1	1.59	-0.47	0.74					0.53	
		5	1.42	-0.46	0.79					0.51	
		10	1.35	-0.45	0.81					0.50	
		20	1.25	-0.44	0.85					0.49	